

1



² Supporting Information for

³ Forecasting range shifts of a dioecious plant species under climate change

⁴ Jacob K. Moutouama, Aldo Compagnoni and Tom E.X. Miller

⁵ Jacob Moutouama.

⁶ E-mail: jmoutouama@gmail.com

⁷ This PDF file includes:

⁸ Supporting text

⁹ Figs. S1 to S23

¹⁰ Table S1

¹¹ SI References

12 **Supporting Information Text**

13 **Supporting Methods**

14 **A. Climatic data collection.** The general circulation models (GCMs) were selected from the Coupled Model Intercomparison
15 Project Phase 5 (CMIP5): Model for Interdisciplinary Research on Climate (MIROC5), Australian Community Climate and
16 Earth System Simulator (ACCESS1-3), Community Earth System Model (CESM1-BGC), Centro Euro-Mediterraneo sui
17 Cambiamenti Climatici Climate Model (CMCC-CM). All the GCMs were also downloaded from Chelsa (1). We evaluated future
18 climate projections from two scenarios of representative concentration pathways (RCPs): RCP4.5, an intermediate-to-pessimistic
19 scenario assuming a radiative forcing amounting to 4.5 W m^{-2} by 2100, and RCP8.5, a pessimistic emission scenario which
20 projects a radiative forcing of 8.5 W m^{-2} by 2100 (2, 3).

21 Projection data for the three 30-year periods included warmer or colder conditions than observed in our experiment, so
22 extending our inferences to these conditions required some extrapolation. However, across all sites, both study years were
23 1–2°C warmer than their corresponding “current” (1990–2019) temperature normals (Fig. S23). Additionally, the 2014–15
24 growing season was generally wetter and cooler across the study region than 2015–16 (Fig. S23). Combined, the geographic
25 and inter-annual replication of the common garden experiment provided good coverage of most past and future conditions
26 throughout the study region (Fig. 1).

27 **B. Sex-specific demographic responses to climatic variation across common garden sites.** Vital rate models were fit with the
28 same linear predictors for the expected value (μ) (Eq. 1):

$$\begin{aligned} \mu = & \beta_0 + \beta_1 \text{size} + \beta_2 \text{sex} + \beta_3 \text{pptgrow} + \beta_4 \text{pptdorm} + \beta_5 \text{tempgrow} + \beta_6 \text{tempdorm} \\ & + \beta_7 \text{pptgrow * sex} + \beta_8 \text{pptdorm * sex} + \beta_9 \text{tempgrow * sex} + \beta_{10} \text{tempdorm * sex} \\ & + \beta_{11} \text{size * sex} + \beta_{12} \text{pptgrow * tempgrow} + \beta_{13} \text{pptdorm * tempdorm} \\ & + \beta_{14} \text{pptgrow * tempgrow * sex} + \beta_{15} \text{pptdorm * tempdorm * sex} + \beta_{16} \text{pptgrow}^2 \\ & + \beta_{17} \text{pptdorm}^2 + \beta_{18} \text{tempgrow}^2 + \beta_{19} \text{tempdorm}^2 + \beta_{20} \text{pptgrow}^2 * \text{sex} \\ & + \beta_{21} \text{pptdorm}^2 * \text{sex} + \beta_{22} \text{tempgrow}^2 * \text{sex} + \beta_{23} \text{tempdorm}^2 * \text{sex} + \phi + \rho + \nu \end{aligned} \quad [1]$$

30 where β_0 is the grand mean intercept, β_1 is the size dependent slopes. size was on a natural logarithm scale. $\beta_2 \dots \beta_{13}$ represent
31 the climate dependent slopes. $\beta_{14} \dots \beta_{23}$ represent the sex-climate interaction slopes. pptgrow is the precipitation of the growing
32 season, tempgrow is the temperature of the growing season, pptdorm is the precipitation of the dormant season, tempdorm is
33 the temperature of the dormant season.

34 All vital rates were fit with second-degree polynomial functions to accommodate the possibility of hump-shaped relationships
35 (reduced demographic performance at both extremes). We also included two-way interactions between sex and each climate
36 driver and between temperature and precipitation within each season, and a three-way interaction between sex, temperature,
37 and precipitation within each season. We modeled survival and flowering data with a Bernoulli distribution and the growth
38 (tiller number) with a zero-truncated Poisson inverse Gaussian distribution. Fertility (panicle count conditional on flowering)
39 was modeled as zero-truncated negative binomial. We used generic, weakly informative priors to fit coefficients for survival,
40 growth, flowering models ($\beta \sim N(0, 1.5)$) and random effect variances ($\sigma \sim \text{Gamma}(\gamma(0.1, 0.1))$). We fit fertility model with
41 also weakly informative priors for coefficients ($\beta \sim N(0, 0.15)$). Different priors were used for fertility because the panicle
42 model has a large number of parameters relative to the amount of available data (subset of our data) and because these
43 specifics priors help prevent the model from overfitting. Each vital rate also includes normally distributed random effects for
44 block-to-block variation ($\phi \sim N(0, \sigma_{\text{block}})$), site to site variation ($\nu \sim N(0, \sigma_{\text{site}})$), and source-to-source variation that is
45 related to the genetic provenance of the transplants used to establish the common garden ($\rho \sim N(0, \sigma_{\text{source}})$).

46 **C. Sex ratio responses to climatic variation across common garden sites.** To understand the impact of climatic variation across
47 common garden sites on sex ratio (OSR and SR), we used bayesian models to propagate the uncertainty in our estimates of the
48 the expected value (ν) (Eq. 2):

$$\begin{aligned} \nu = & \omega_0 + \omega_1 \text{pptgrow} + \omega_2 \text{pptdorm} + \omega_3 \text{tempgrow} + \omega_4 \text{tempdorm} + \\ & \omega_5 \text{pptgrow}^2 + \omega_6 \text{pptdorm}^2 + \omega_7 \text{tempgrow}^2 + \omega_8 \text{tempdorm}^2 + \epsilon \end{aligned} \quad [2]$$

50 where OSR is the proportion of panicles that were female or proportion of female individuals in the experimental populations,
51 c is the climate. ω_0 is the intercept, $\omega_1, \dots, \omega_8$ are the climate dependent slopes. ϵ is error term.

52 We modeled the OSR and SR data with a Bernoulli distribution and used non informative priors for each coefficient
53 ($\omega \sim N(0, 100)$).

54 **D. Sex ratio experiment.** To estimate the probability of seed viability, the germination rate and the effect of sex-ratio variation
55 on female reproductive success, we conducted a sex-ratio experiment at one site near the center of the range to estimate
56 the effect of sex-ratio variation on female reproductive success. The details of the experiment are provided in (4) and (5).
57 Here we provide a summary of the experiment. We established 124 experimental populations in plots measuring 0.4 x 0.4m
58 and separated by at least 15m from each other. We varied population density (1–48 plants/plot) and sex ratio (0%–100%.

59 female) across the experimental populations, and we replicated 34 combinations of density and sex ratio. We collected panicles
60 from a subset of females in each plot and recorded the number of seeds in each panicle. We assessed reproductive success
61 (seeds fertilized) using greenhouse-based germination and trazolium-based seed viability assays. Seed viability was modeled to
62 propagate the uncertainty in our estimates with a binomial distribution where the probability of viability (v) was given by:

63
$$v = v_0 * (1 - OSR^\alpha) \quad [3]$$

64 where OSR is the proportion of panicles that were female in the experimental populations. α is the parameter that control for
65 how viability declines with increasing female bias. Further, germination rate was modeled using a binomial distribution to
66 model the germination data from greenhouse trials. Given that germination was conditional on seed viability, the probability
67 of success was given by the product $v * g$, where v is a function of OSR (Eq. 3) and g is assumed to be constant.

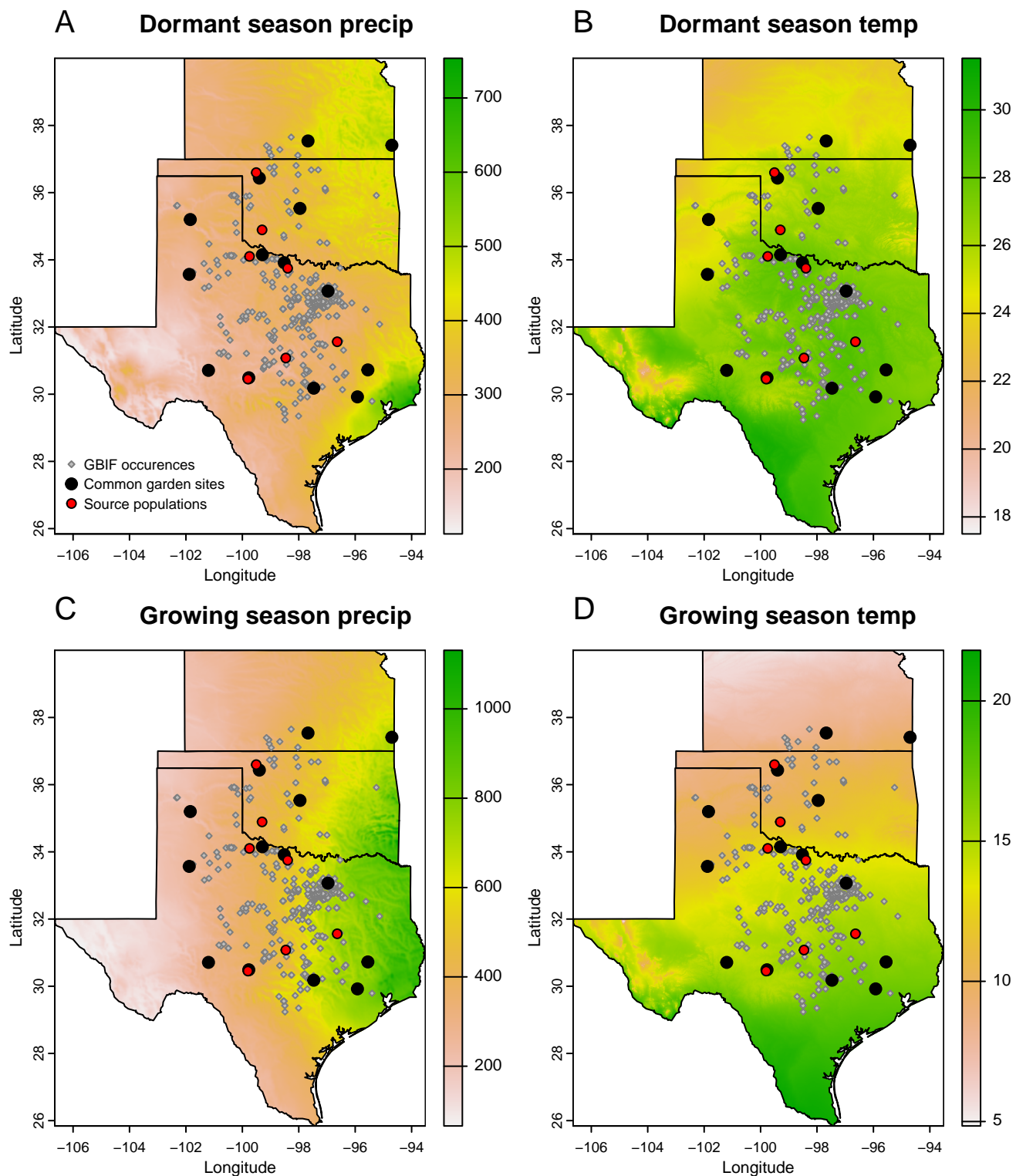


Fig. S1. texbfMaps of 30-year (1990–2019) climate normals and study sites used for demographic monitoring of *Poa arachnifera* in Texas, Kansas and Oklahoma in the United States. Precipitation is in mm and temperature is in °C. We surveyed 22 natural populations (grey diamond). The common garden sites were installed on 14 sites (black circle) collected from 7 source populations (red circle)

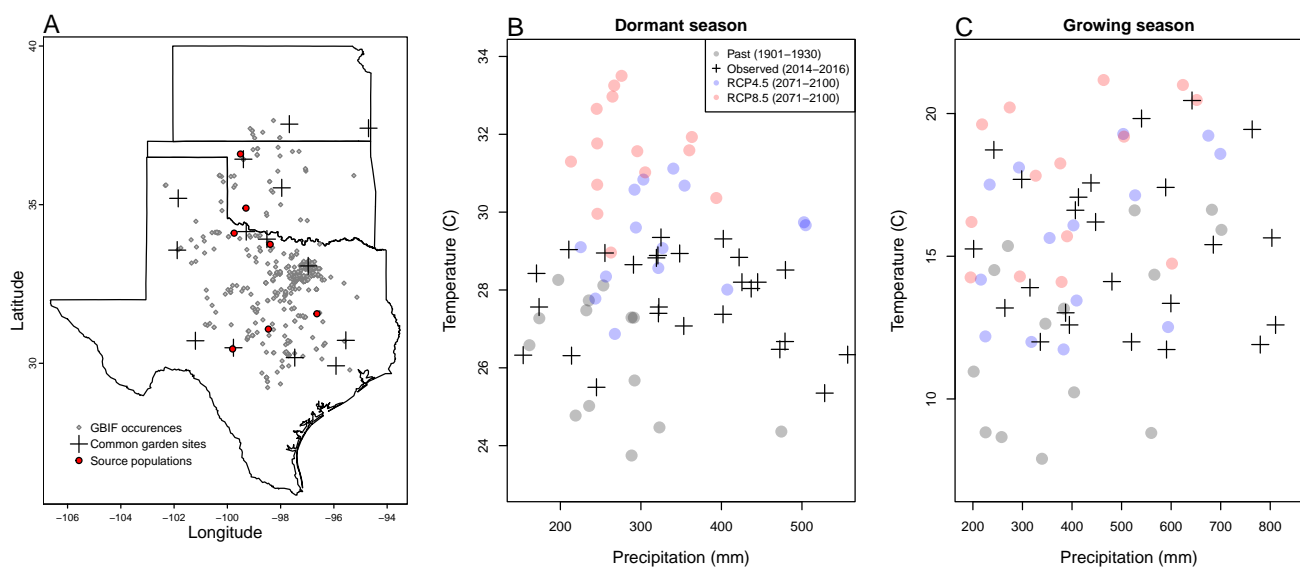


Fig. S2. Experimental gardens and climate of the study region. **A:** Map of 14 experimental garden sites (crosses) in Texas, Oklahoma, and Kansas relative to GBIF occurrences of *Poa arachnifera* (gray points). Red points indicate source populations for plants used in the common garden experiment. **B,C:** Past, future, and observed climate space for growing and dormant seasons. Crosses show observed conditions for the sites and years of the common garden experiment. Gray points show historical (1901–1930) climate normals, and blue and red points show end-of-century (2071–2100) climate normals for RCP4.5 and RCP8.5 projections, respectively, from MIROC5.

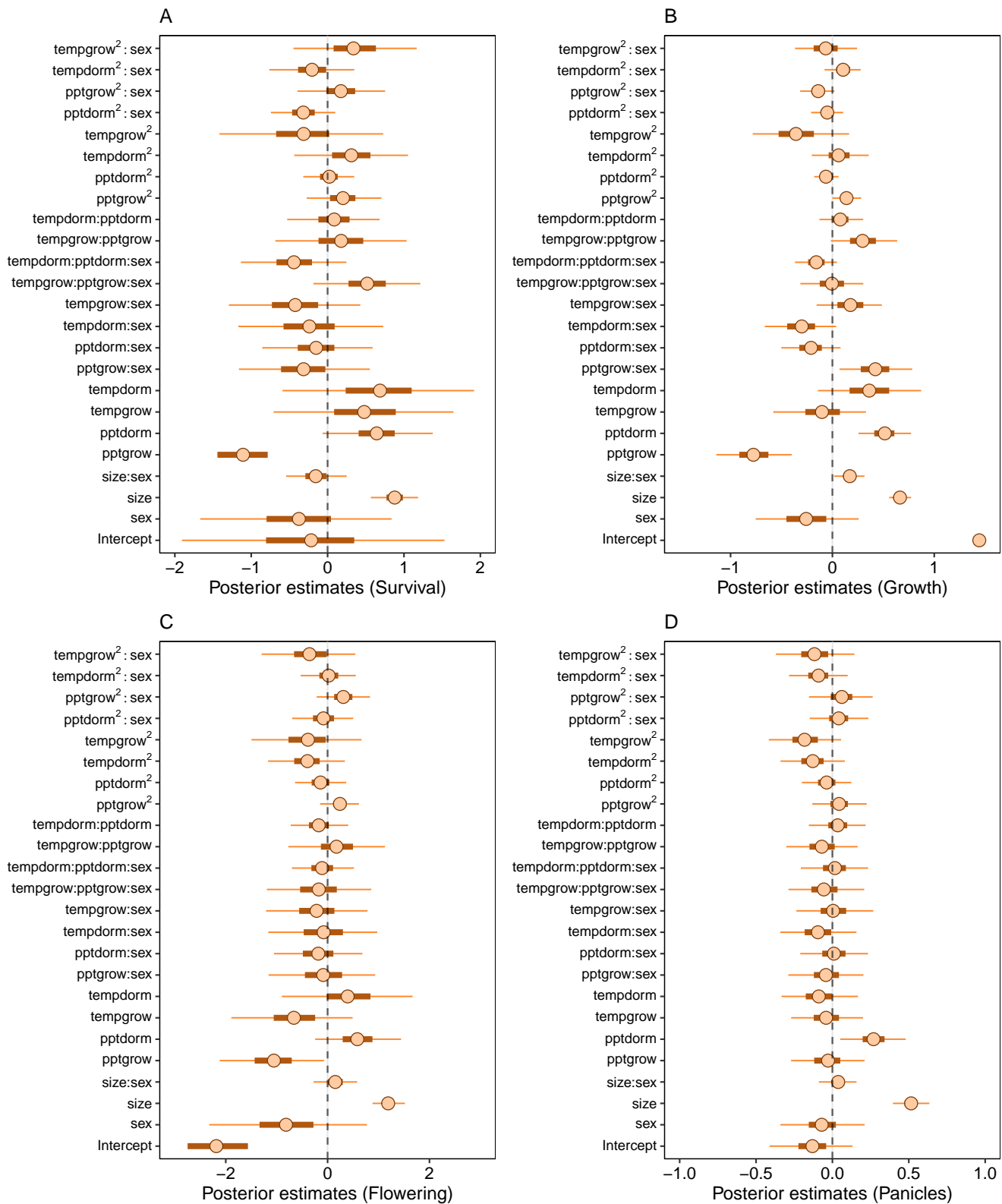


Fig. S3. Mean parameter values, 50% and 95% credible intervals of the posterior probability distributions. pptgrow is the precipitation of growing season, Tempgrow is the temperature of growing season, pptdorm is the temperature of dormant season, Tempdorm is the temperature of dormant season.

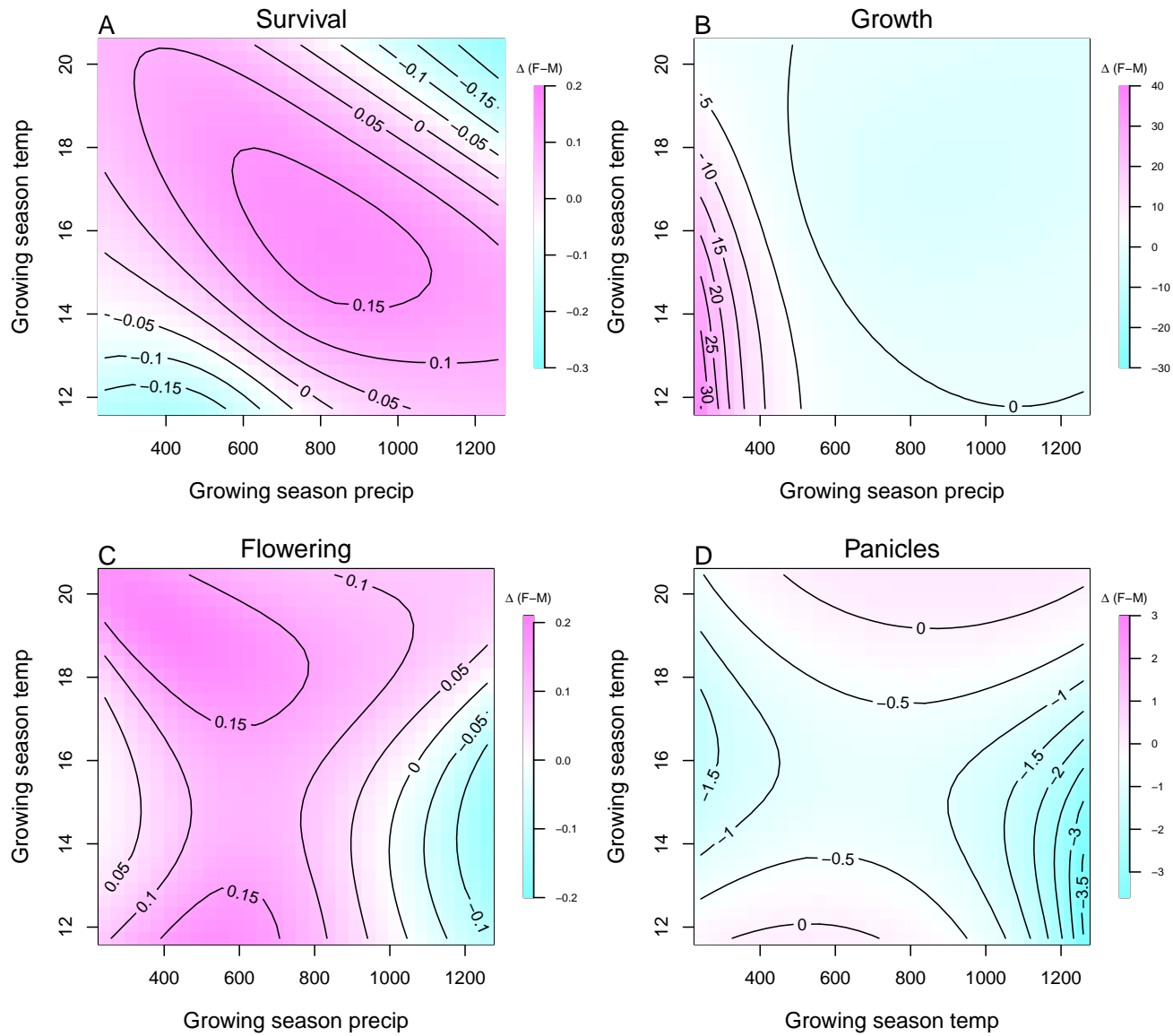


Fig. S4. Predicted difference in demographic response to climate across species range between female and male. Contours show predicted value of that difference conditional on precipitation and temperature of growing season

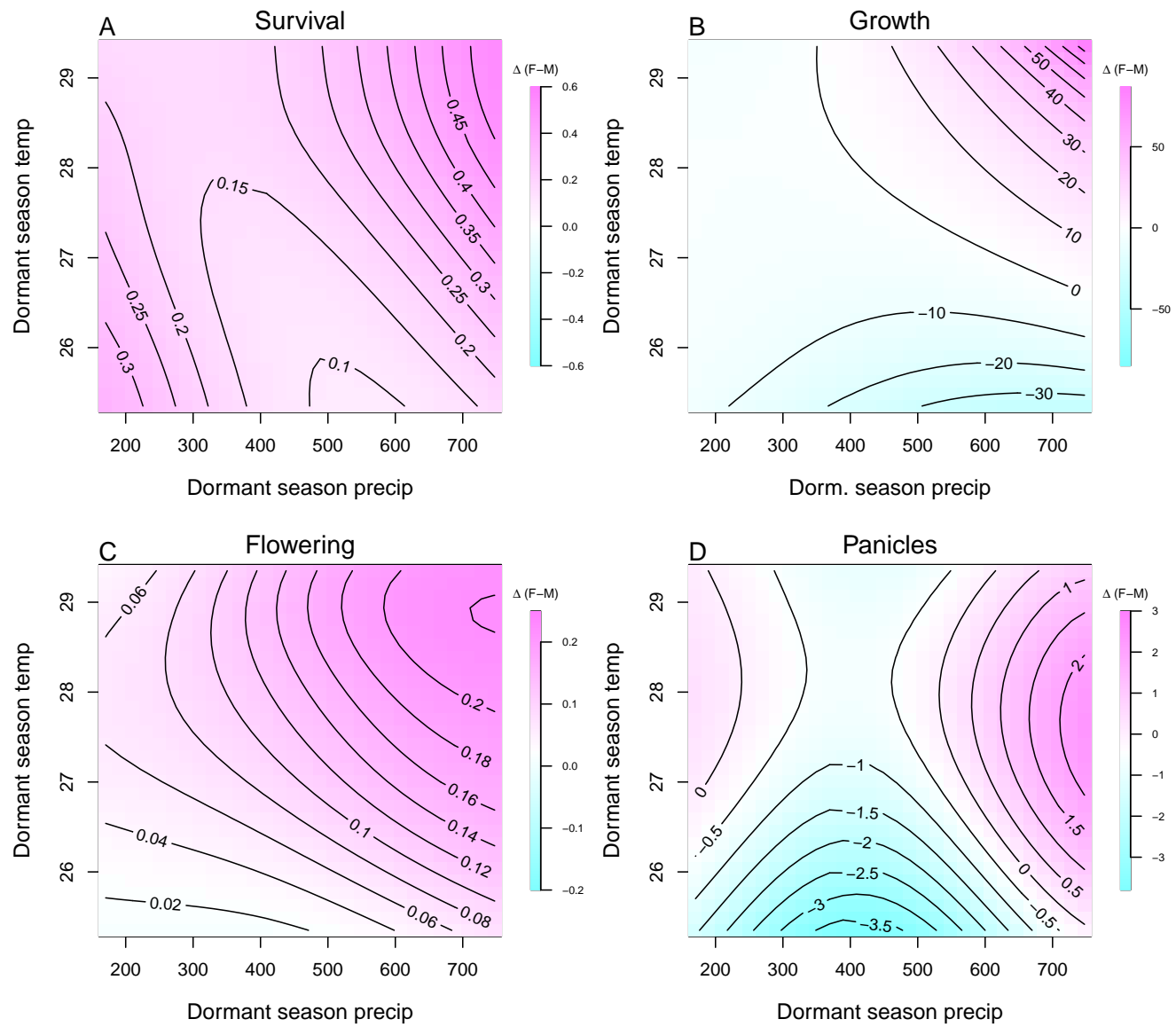


Fig. S5. Predicted difference in demographic response to climate across species range between female and male. Contours show predicted value of that difference conditional on precipitation and temperature of the dormant season

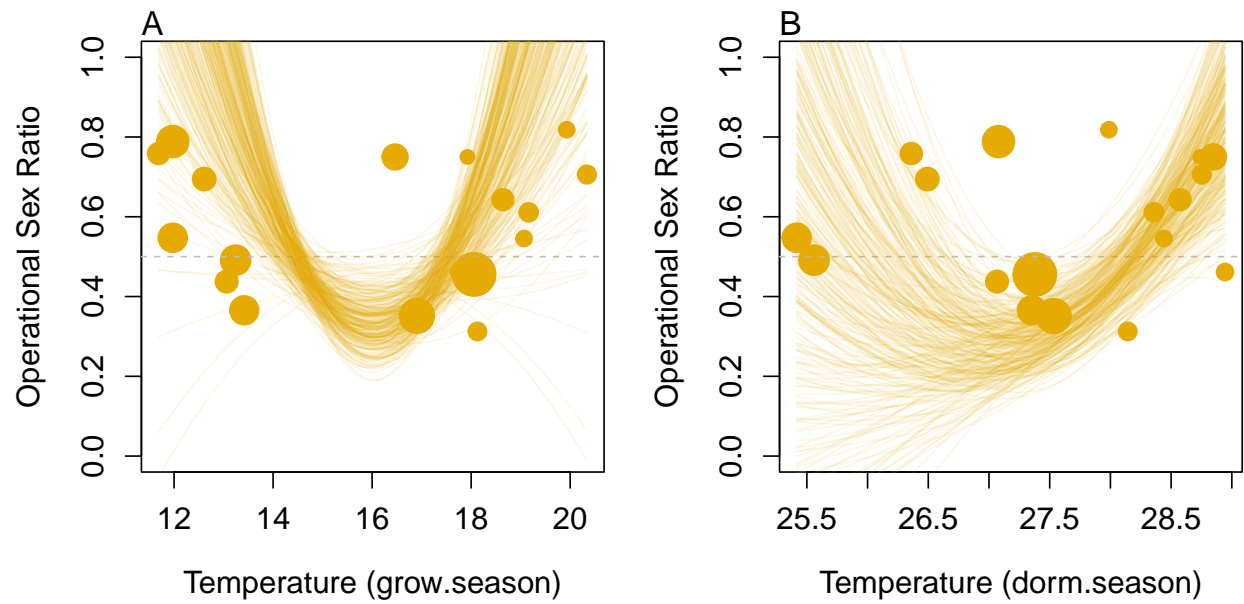


Fig. S6. Significant Operational Sex Ratio response across climate gradient. (A, B) Proportion of panicles that were females across temperature of the growing and dormant season. Each line represents a posterior sample. We used (300 posterior samples)

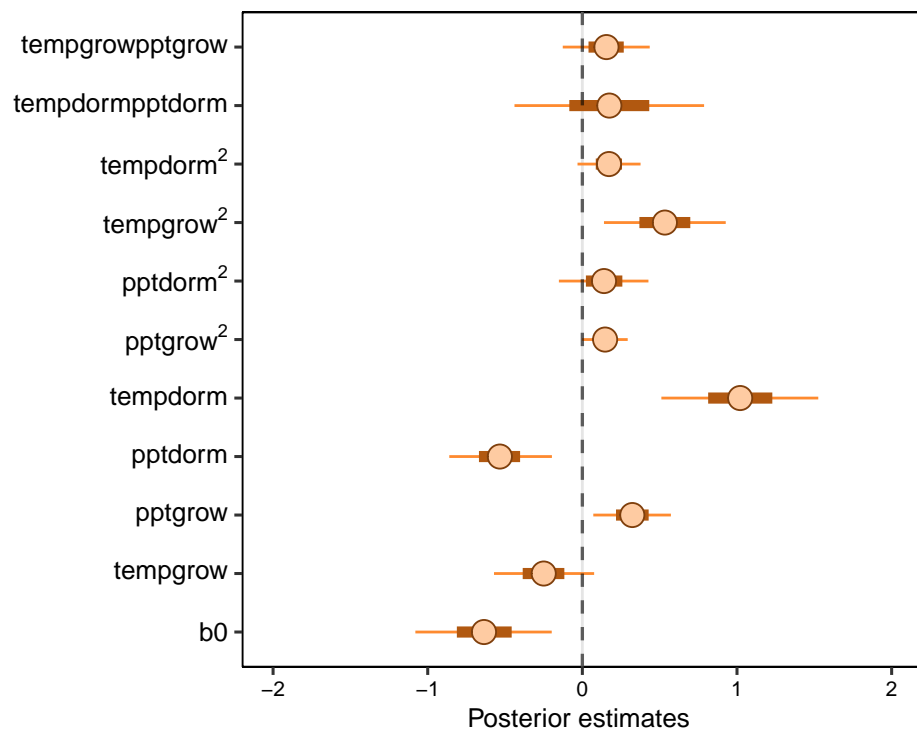


Fig. S7. Mean parameter values, 50% and 95% credible intervals of the posterior probability distributions for climate drivers of operational sex ratio (female fraction of total panicles) across common garden years and sites. pptgrow is the precipitation of growing season, Tempgrow is the temperature of growing season, pptdorm is the temperature of dormant season, Tempdorm is the temperature of dormancy.

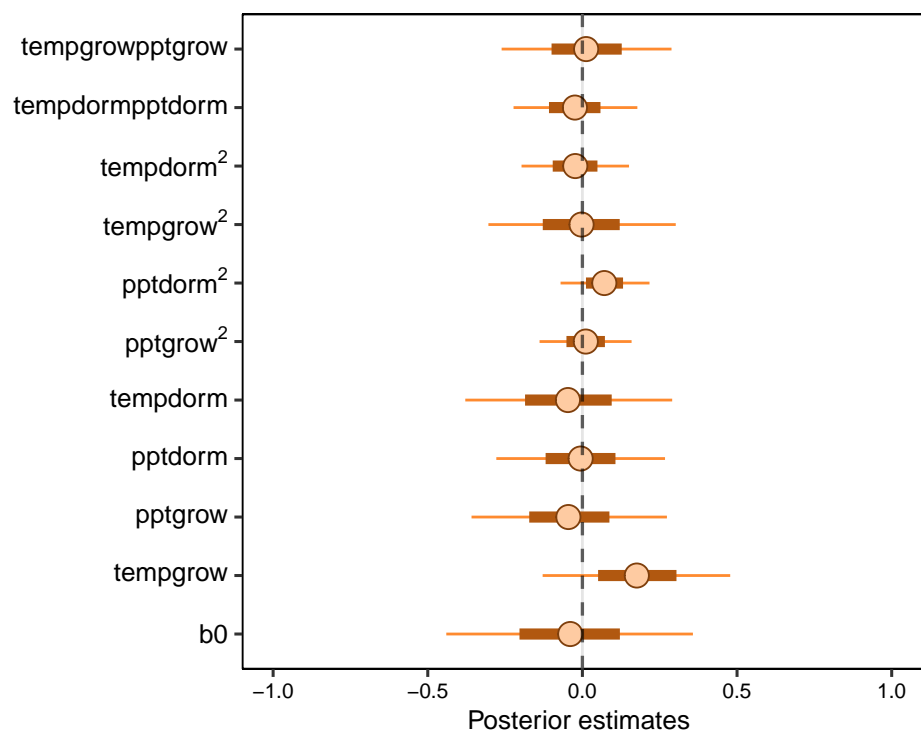


Fig. S8. Mean parameter values, 50% and 95% credible intervals of the posterior probability distributions for climate drivers of sex ratio (female fraction of the populations) across common garden years and sites. pptgrow is the precipitation of growing season, Tempgrow is the temperature of growing season, pptdorm is the temperature of dormant season, Tempdorm is the temperature of dormancy season.

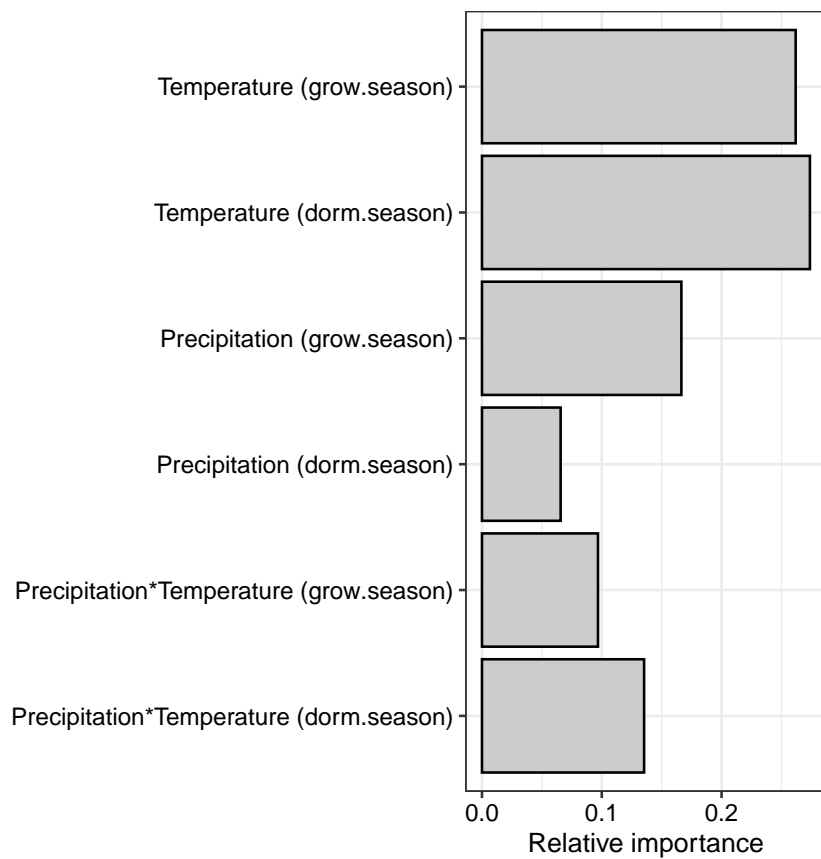


Fig. S9. Life Table Response Experiment: The bar represent the relative importance of each predictors.

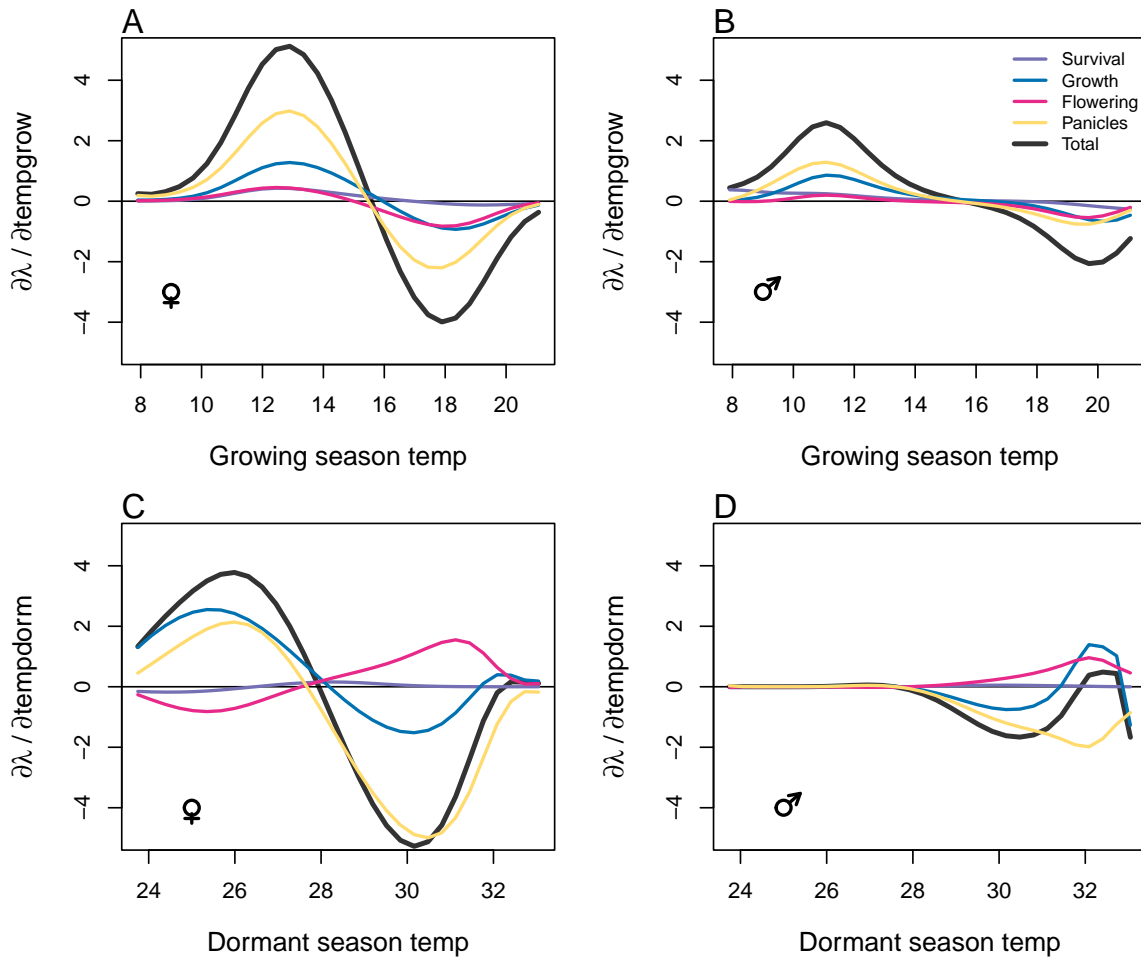


Fig. S10. Life table response experiment decomposition of the sensitivity of λ to seasonal climate into additive vital rate contributions of males and females based on posterior mean parameter estimates. (A) Temperature of growing season (contribution of female), (B) Temperature of growing season (contribution of male), (C) Temperature of dormant season (contribution of female) and (D) Temperature of dormant season (contribution of male).

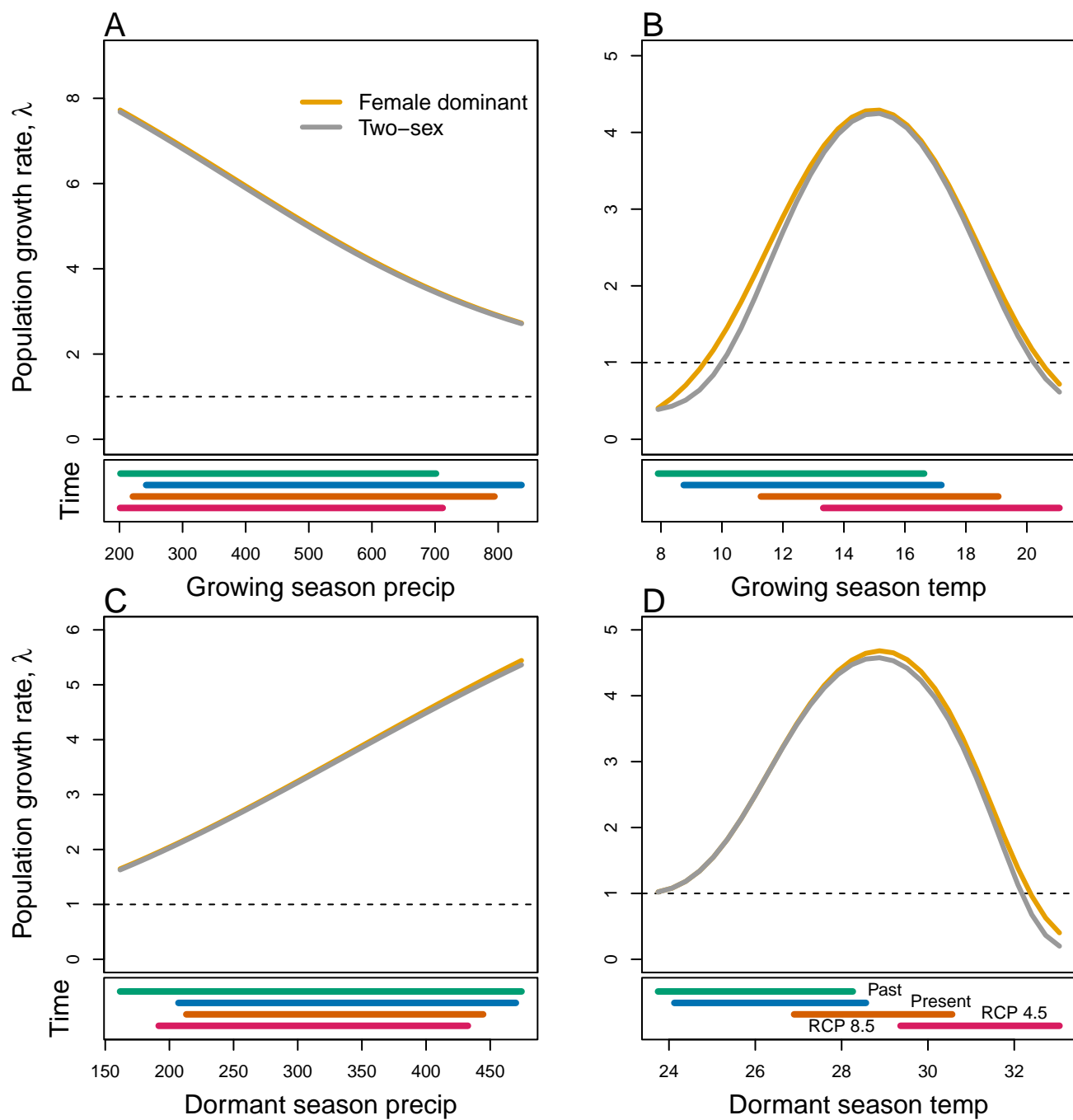


Fig. S11. Predicted population growth rate (λ) in different ranges of climate. (A) Precipitation of the growing season, (B) Temperature of the growing season, (C) Precipitation of the dormant season, (D) Temperature of the dormant season. The grey curve shows prediction by the two-sex matrix projection model that incorporates sex-specific demographic responses to climate with sex ratio dependent seed fertilization. The orange curve represents the prediction by the female dominant matrix projection model. The dashed horizontal line indicates the limit of population viability ($\lambda = 1$). Lower panels below each data panel show ranges of climate values for different time period (past climate, present and future climates). For future climate, we show a Representation Concentration Pathways (RCP) 4.5 and 8.5. Values population viability of (λ) are derived from the mean climate variables across 4 GCMs (MIROC5, ACCESS1-3, CESM1-BGC, CMCC-CM).

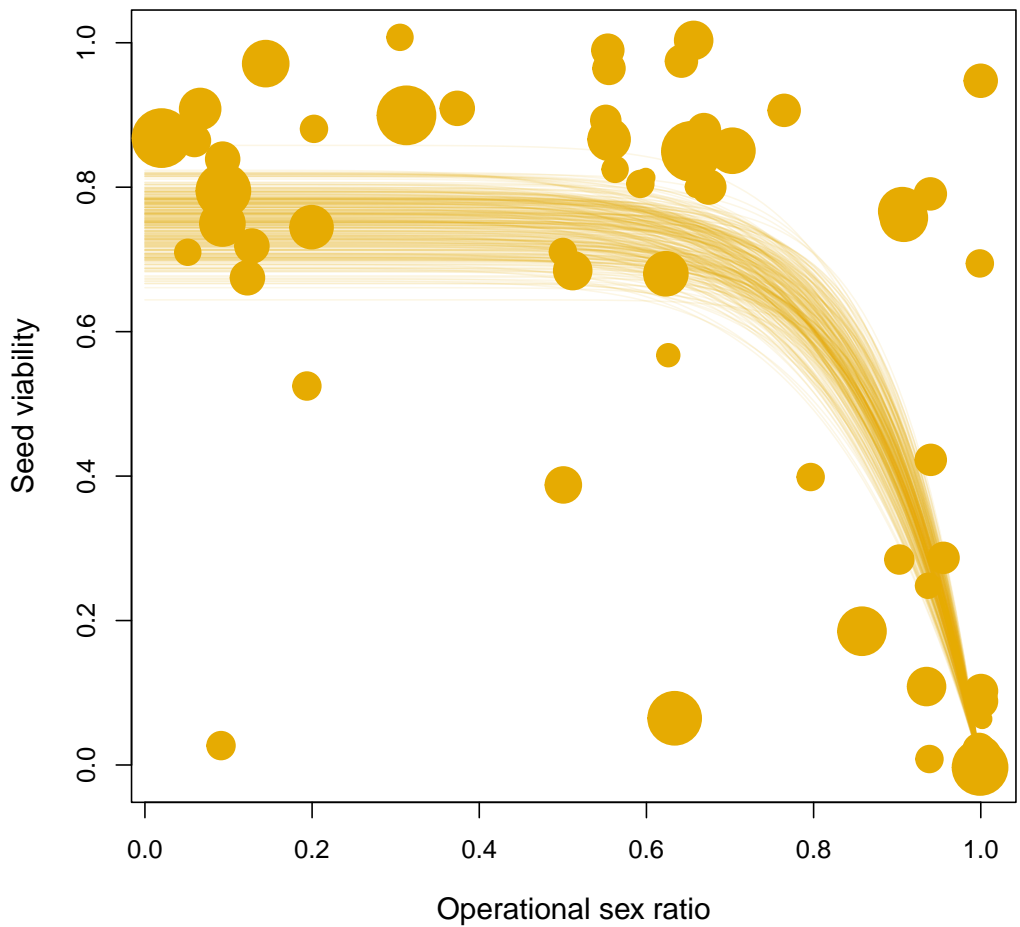


Fig. S12. Seed fertilization success as a function of operational sex ratio (fraction of panicles that are female) in experimental populations. Circles show data from tetrazolium assays of seed viability; circle size is proportional to the number of seeds tested (minimum: 14; maximum: 57). Lines show model predictions for 300 samples from the posterior distribution of parameter estimate

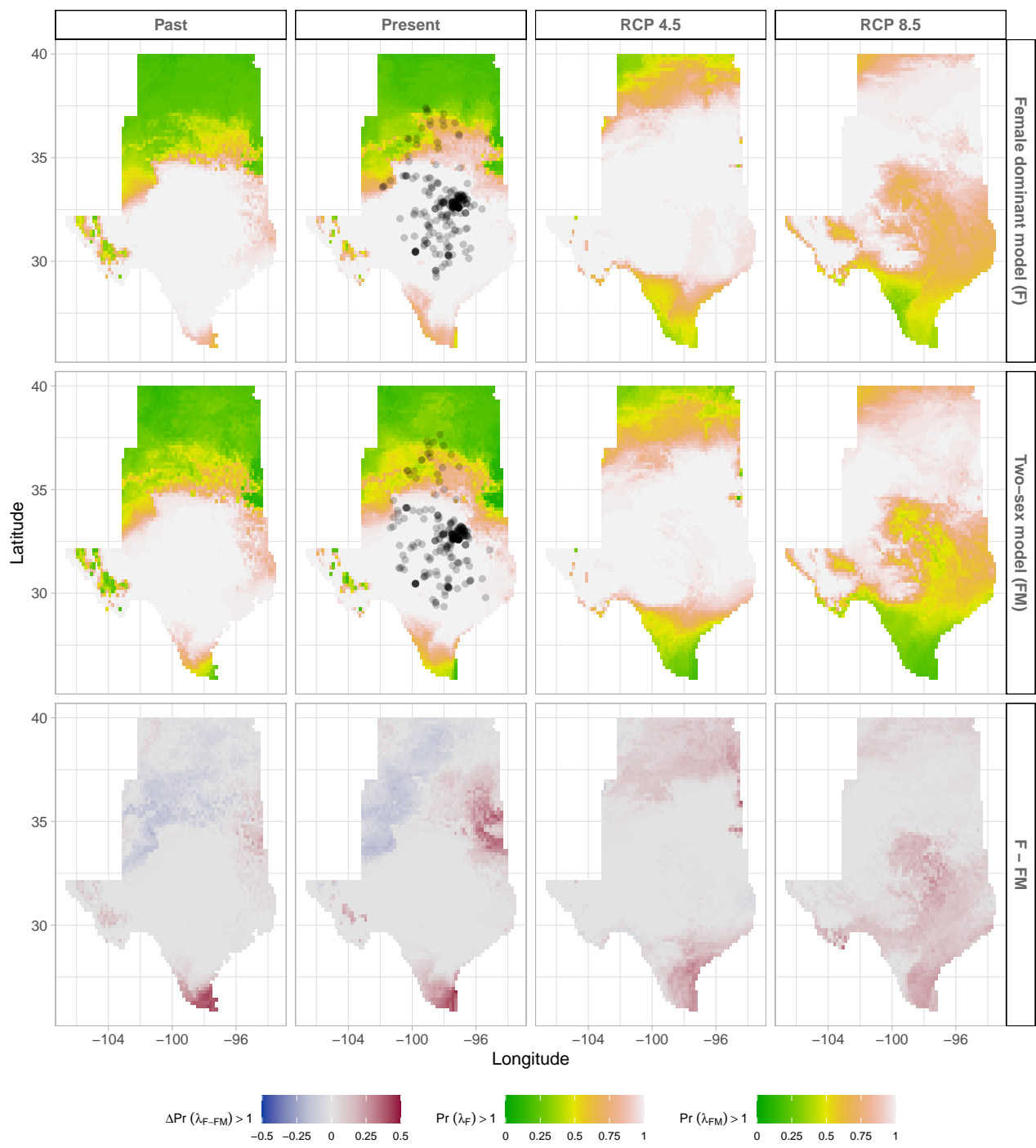


Fig. S13. Climate change favors range shift toward the North edge of the current range. (A) Past, (B) Current, (C and D) Future predicted range shift based on the predicted probabilities of self- sustaining populations, $\Pr(\lambda > 1)$, using the two-sex model that incorporates sex- specific demographic responses to climate with sex ratio dependent seed fertilization. (E) Past, (F) Current, (G and H) Future predicted range shift based on the predicted probabilities of self- sustaining populations, $\Pr(\lambda > 1)$, using the female dominant model. Future projections were based on the CESM1-BGC model. The black dots on panel B and F indicate all known presence points collected from GBIF from 1990 to 2019, which corresponds to the current condition in our prediction. The occurrences of GBIFs are distributed in with higher population fitness habitat $\Pr(\lambda > 1)$, confirming that our study approach can reasonably predict range shifts.

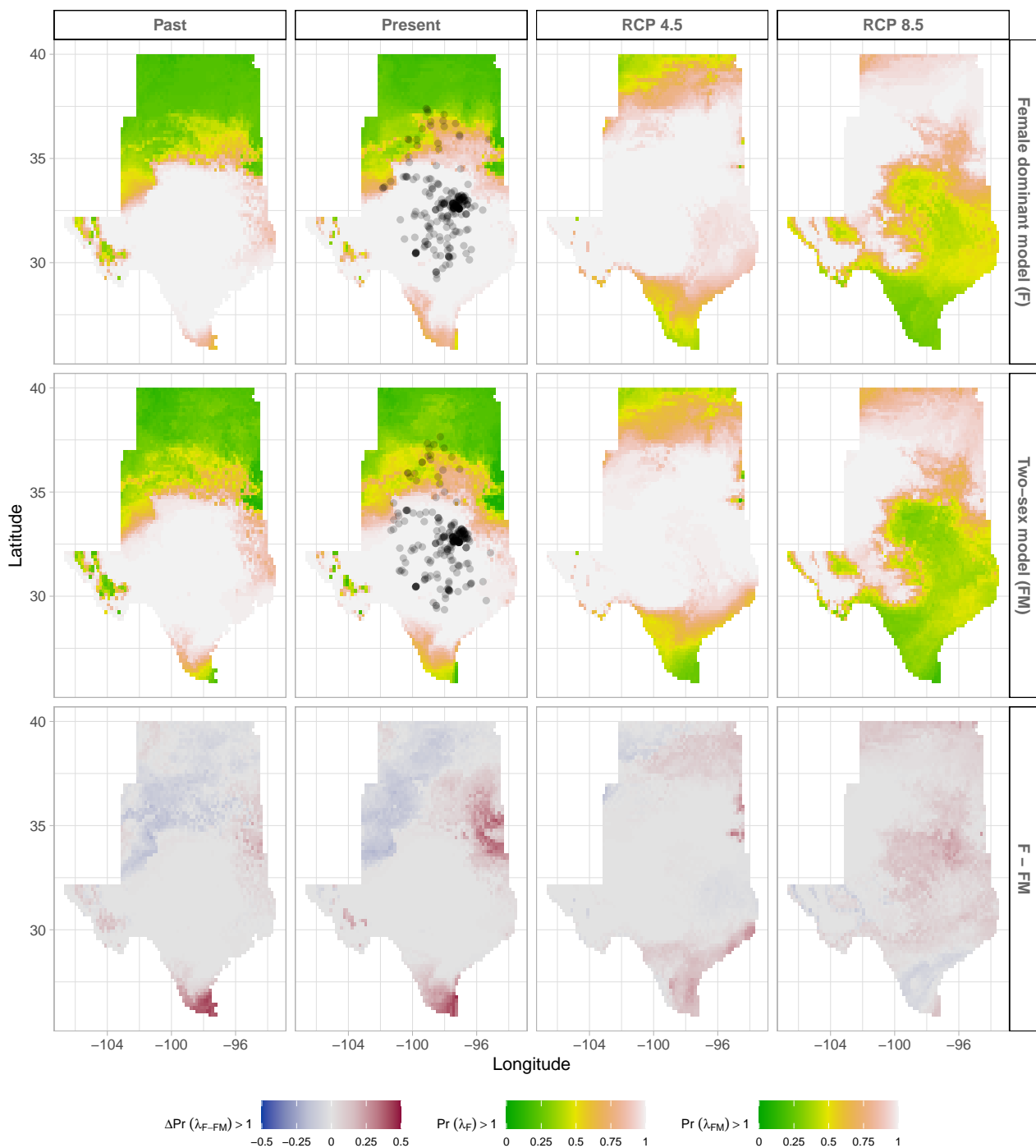


Fig. S14. Climate change favors range shift toward the North edge of the current range. (A) Past, (B) Current, (C and D) Future predicted range shift based on the predicted probabilities of self-sustaining populations, $\Pr(\lambda > 1)$, using the two-sex model that incorporates sex-specific demographic responses to climate with sex ratio dependent seed fertilization. (E) Past, (F) Current, (G and H) Future predicted range shift based on the predicted probabilities of self-sustaining populations, $\Pr(\lambda > 1)$, using the female dominant model. Future projections were based on the ACCESS model. The black dots on panel B and F indicate all known presence points collected from GBIF from 1990 to 2019, which corresponds to the current condition in our prediction. The occurrences of GBIFs are distributed in with higher population fitness habitat $\Pr(\lambda > 1)$, confirming that our study approach can reasonably predict range shifts.

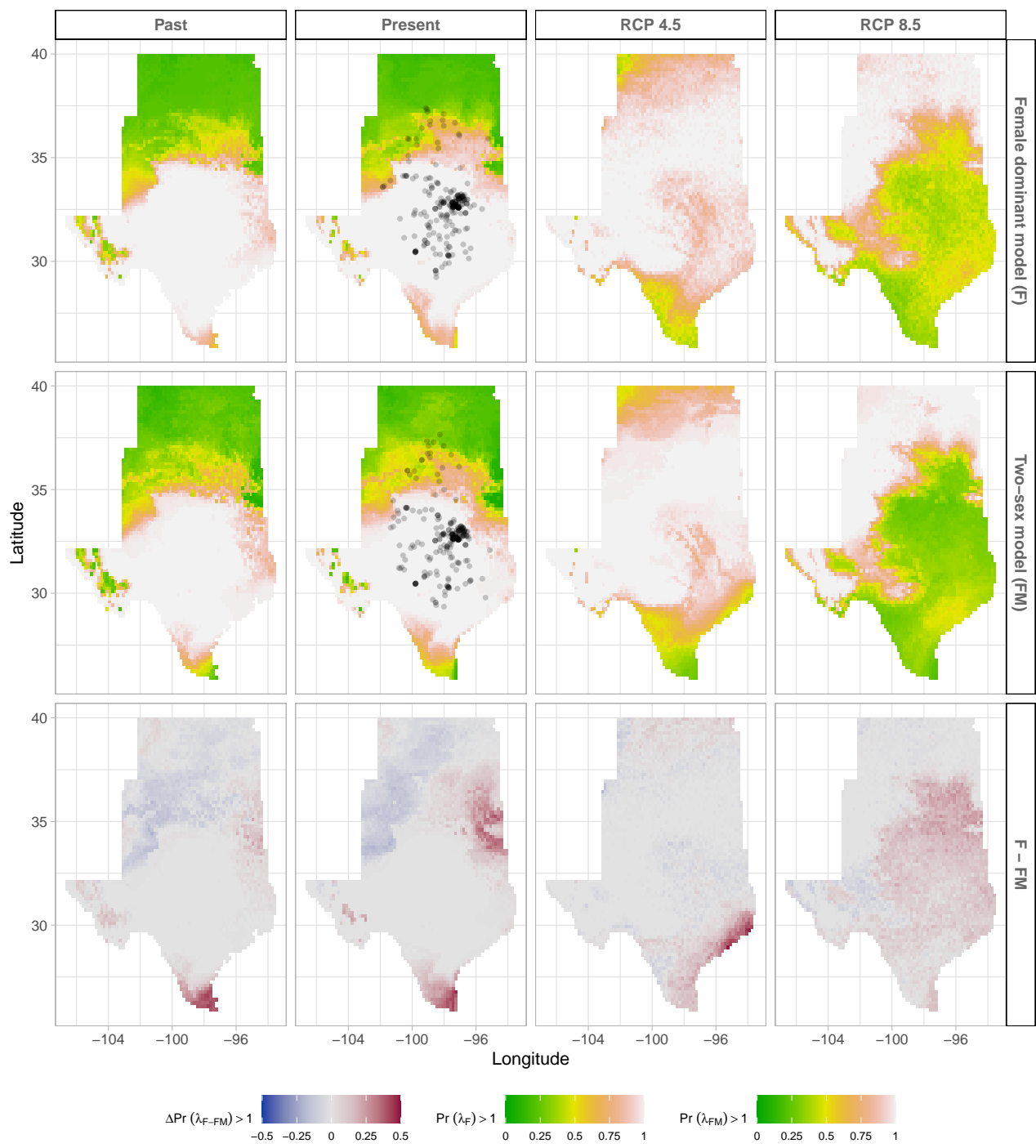


Fig. S15. Climate change favors range shift toward the North edge of the current range. (A) Past, (B) Current, (C and D) Future predicted range shift based on the predicted probabilities of self-sustaining populations, $\text{Pr}(\lambda > 1)$, using the two-sex model that incorporates sex-specific demographic responses to climate with sex ratio dependent seed fertilization. (E) Past, (F) Current, (G and H) Future predicted range shift based on the predicted probabilities of self-sustaining populations, $\text{Pr}(\lambda > 1)$, using the female dominant model. Future projections were based on the MIROC5 model. The black dots on panel B and F indicate all known presence points collected from GBIF from 1990 to 2019, which corresponds to the current condition in our prediction. The occurrences of GBIFs are distributed in higher population fitness habitat $\text{Pr}(\lambda > 1)$, confirming that our study approach can reasonably predict range shifts.

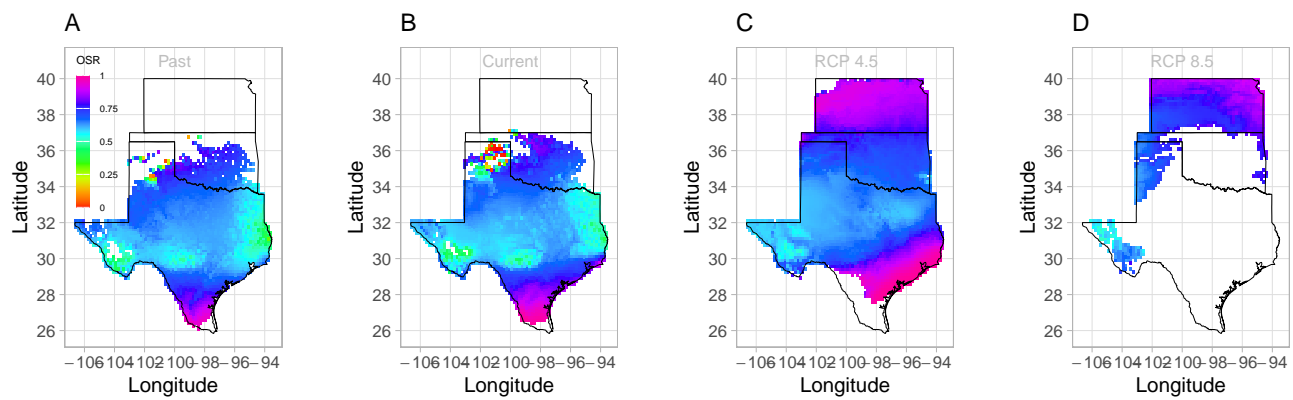


Fig. S16. Projection of Operational Sex Ratio (proportion of female panicle) over time (past, present, future) across species range. Future projections were based on the CMCC-CM model.

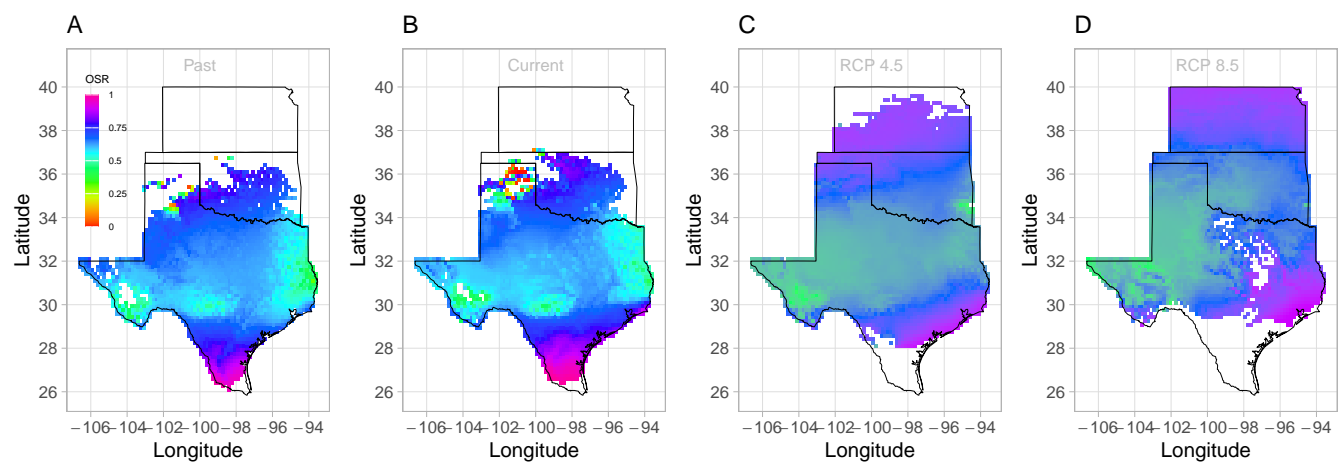


Fig. S17. Projection of in Operational Sex Ratio (proportion of female panicle) over time (past, present, future) across species range. Future projections were based on the CES model.

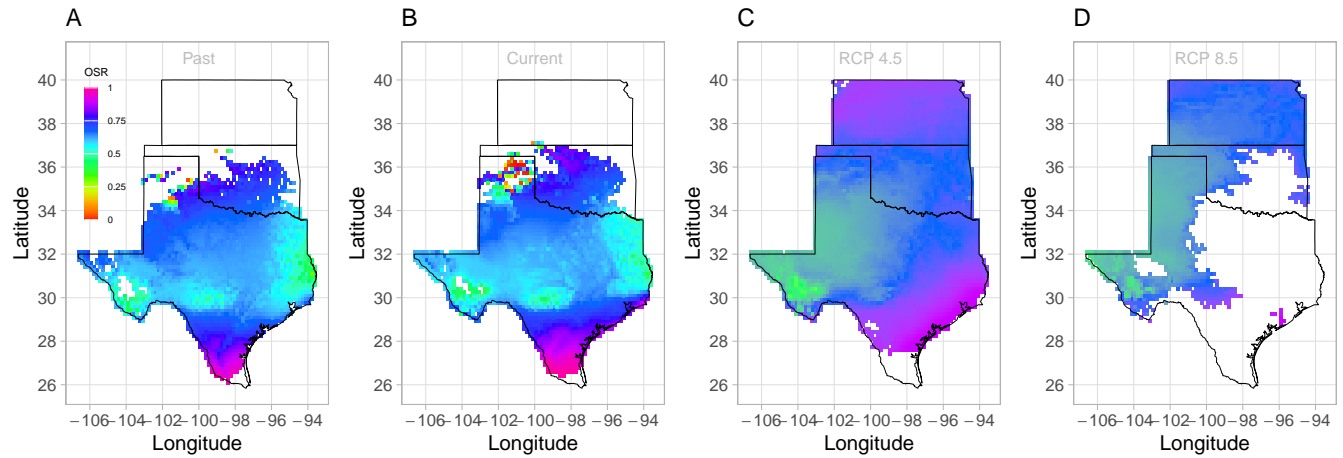


Fig. S18. Projection of Operational Sex Ratio (proportion of female panicle) over time (past, present, future) across species range. Future projections were based on the MIROC model.

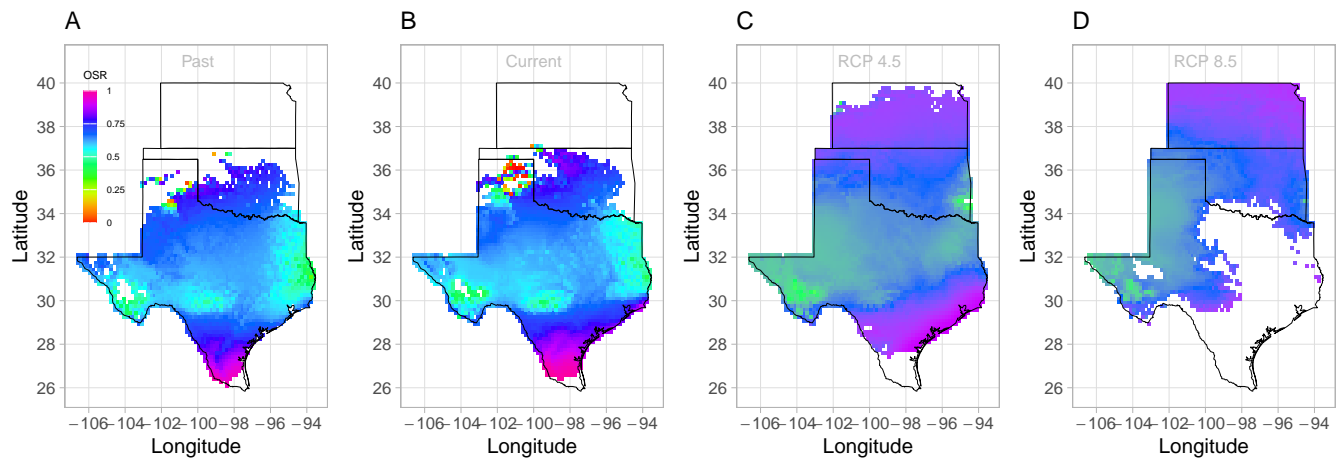


Fig. S19. Projection of Operational Sex Ratio (proportion of female panicle) over time (past, present, future) across species range. Future projections were based on the ACCESS model. The mean sex ratio for each time period is shown as vertical dashed line.

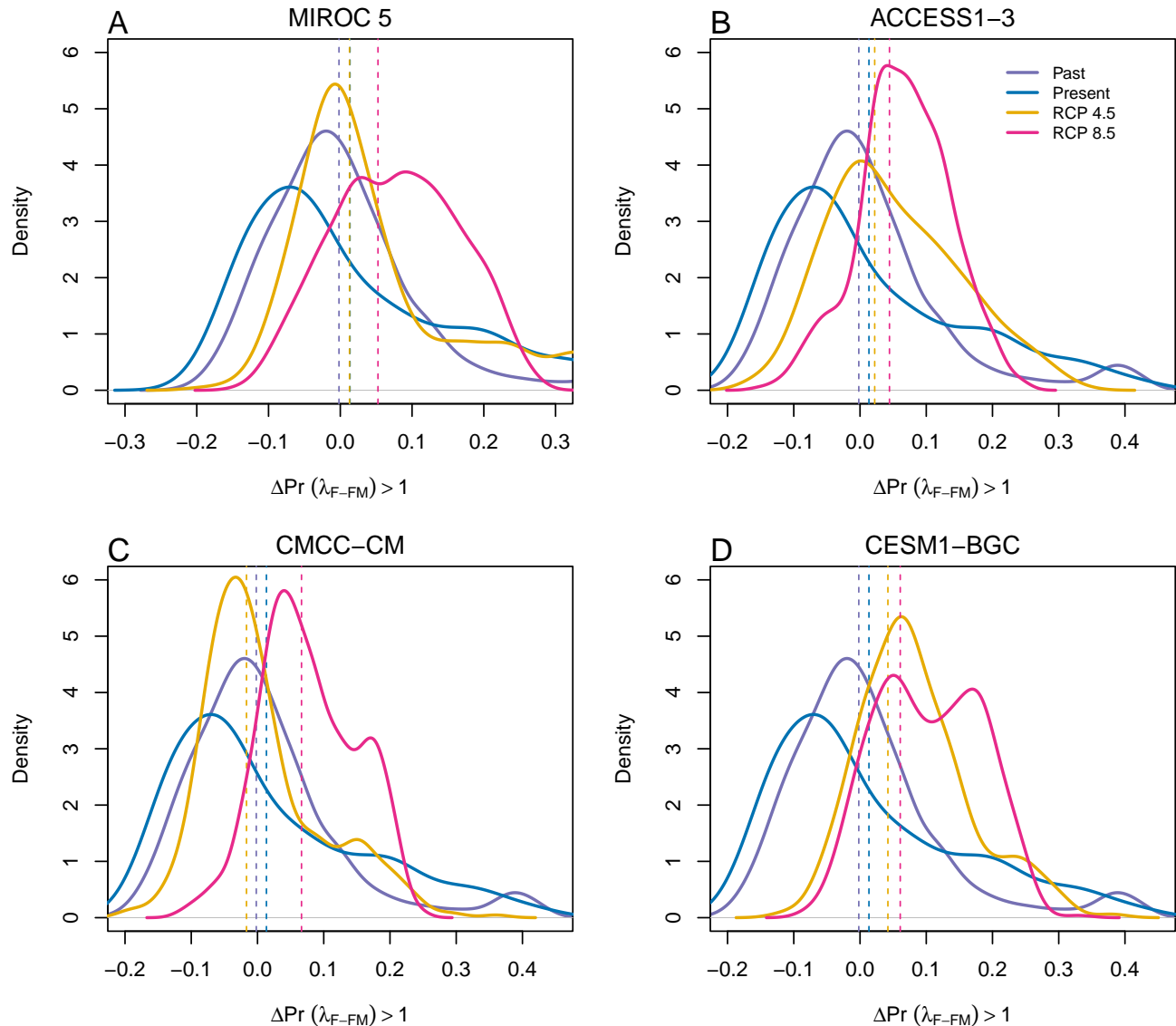


Fig. S20. Assessment of the statistical difference between the two-sex models and the female dominant model across and beyond species range for 4 GCMs. The means for each model are shown as vertical dashed lines.

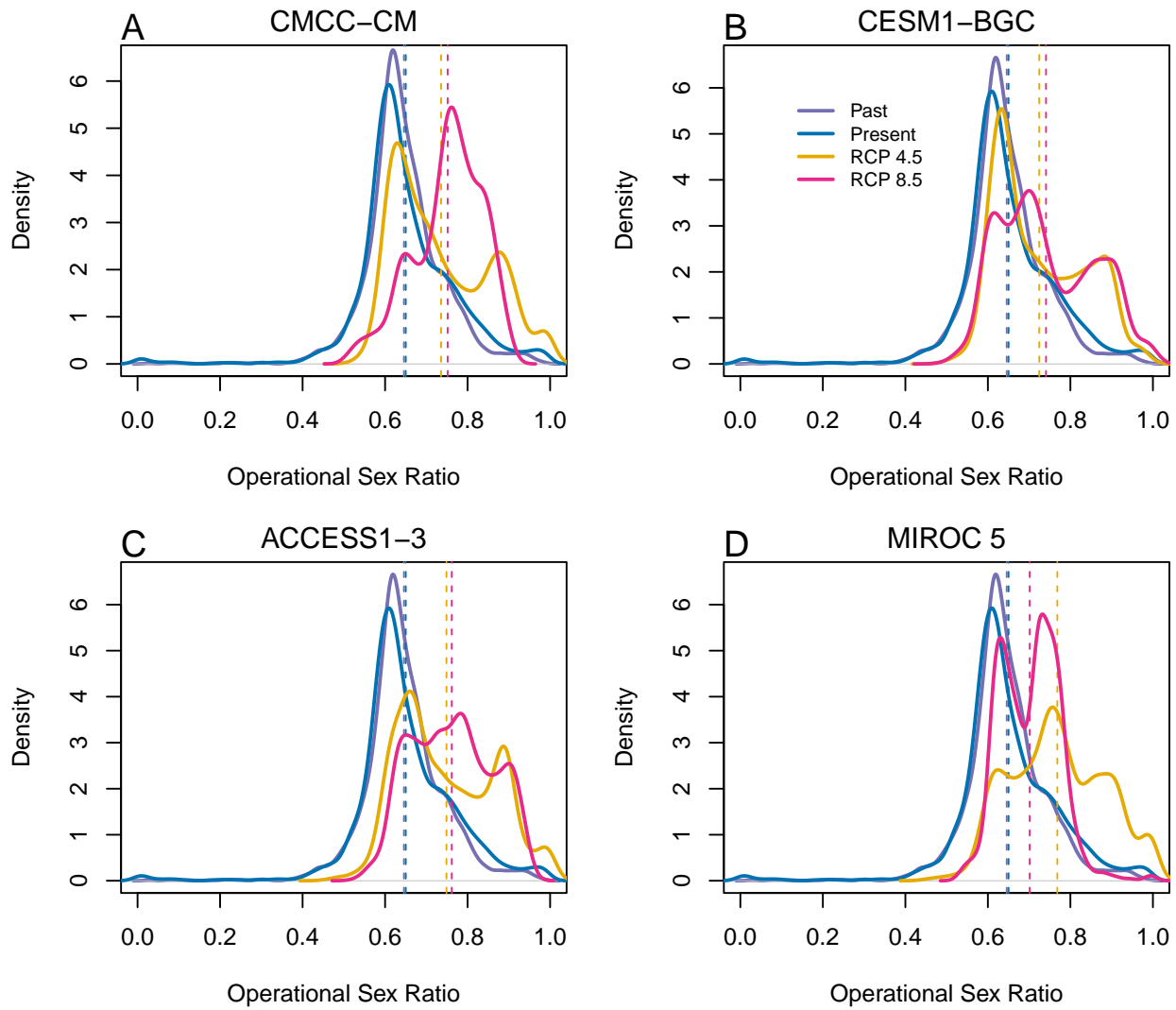


Fig. S21. Change in Operational Sex Ratio (proportion of female) over time (past, present, future). Future projections were based on A) MIROC 5, B) CES, C) ACC. The means for each model are shown as vertical dashed lines.

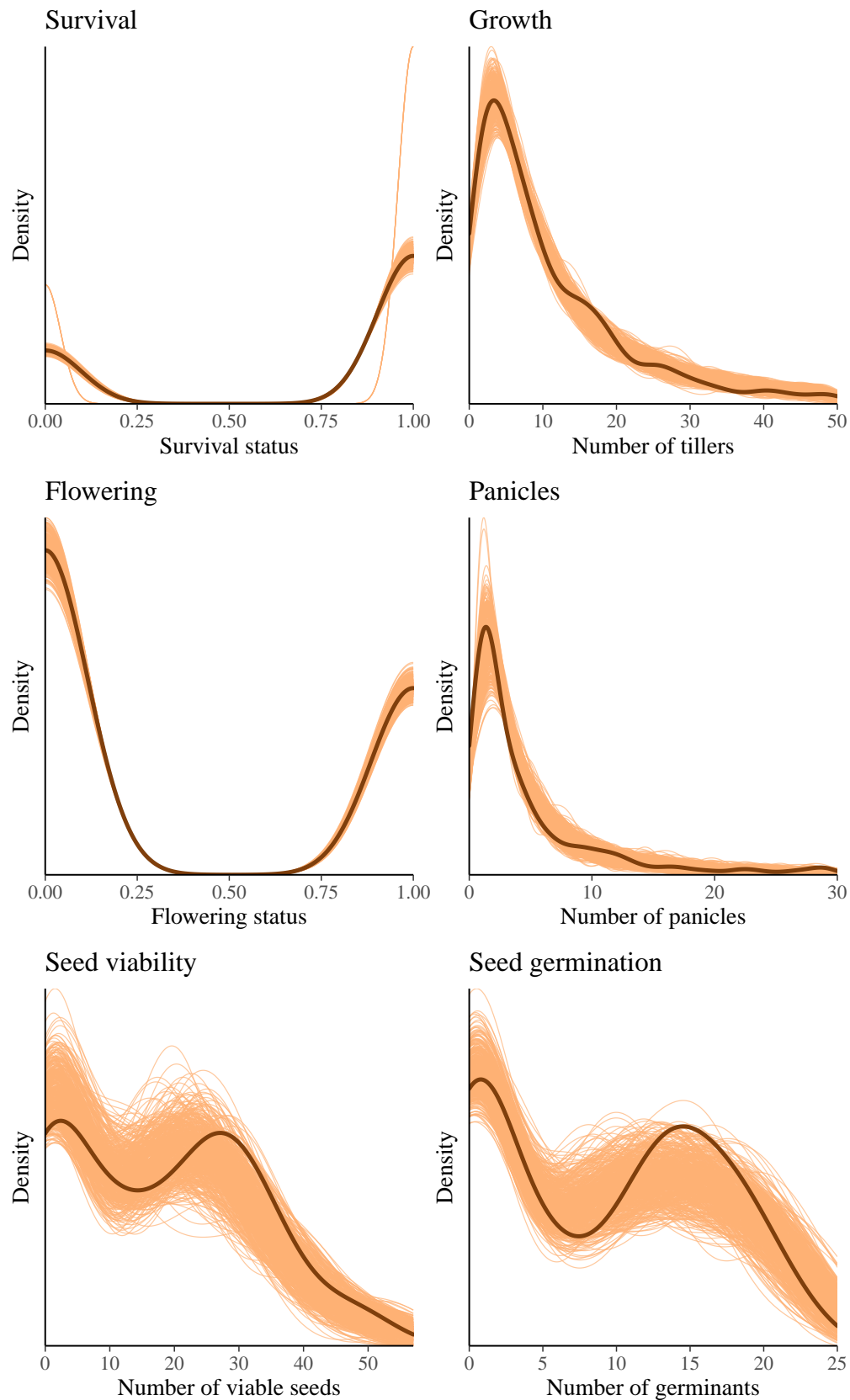


Fig. S22. Posterior predictive checks. Consistency between real data and simulated values suggests that the fitted vital rate models accurately describes the data. Graph shows density curves for the observed data (light orange) along with the simulated values (dark orange).

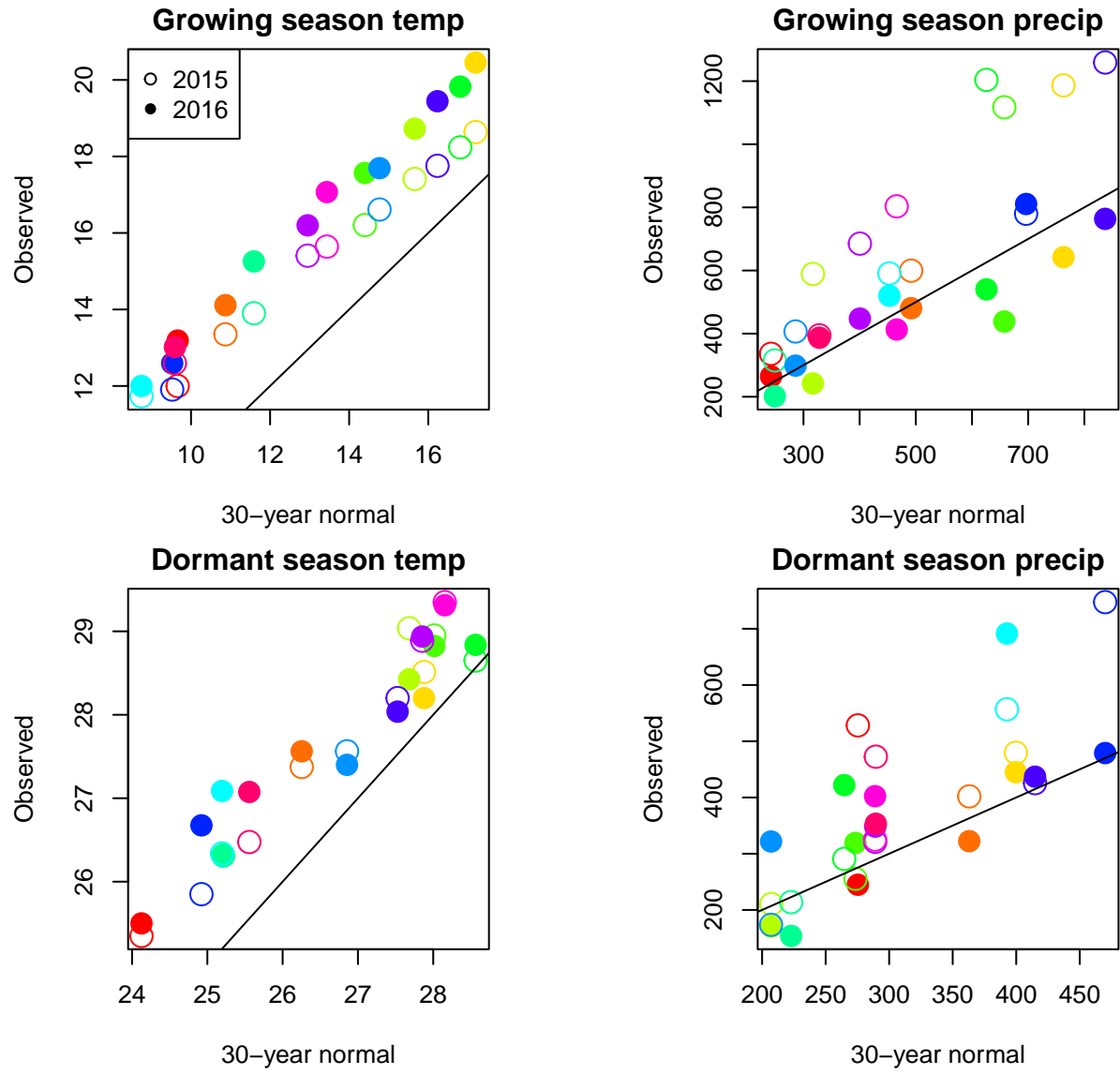


Fig. S23. Comparison of 30-year (1990–2019) climate normals and observed weather conditions at common garden sites during the 2014–15 and 2015–16 census periods. Temperature is in °C and precipitation is in mm. Colors represent sites and lines show the $y = x$ relationship.

69 **Supporting Table**

70 **References**

- 71 1. Benjamin M Sanderson, Reto Knutti, and Peter Caldwell. A representative democracy to reduce interdependency in a
72 multimodel ensemble. *Journal of Climate*, 28(13):5171–5194, 2015.
- 73 2. Allison M Thomson, Katherine V Calvin, Steven J Smith, G Page Kyle, April Volke, Pralit Patel, Sabrina Delgado-Arias,
74 Ben Bond-Lamberty, Marshall A Wise, Leon E Clarke, et al. Rcp4. 5: a pathway for stabilization of radiative forcing by
75 2100. *Climatic change*, 109:77–94, 2011.
- 76 3. Christopher R Schwalm, Spencer Glendon, and Philip B Duffy. Rcp8. 5 tracks cumulative co2 emissions. *Proceedings of the*
77 *National Academy of Sciences*, 117(33):19656–19657, 2020.
- 78 4. Aldo Compagnoni, Kenneth Steigman, and Tom EX Miller. Can't live with them, can't live without them? balancing
79 mating and competition in two-sex populations. *Proceedings of the Royal Society B: Biological Sciences*, 284(1865):20171999,
80 2017.
- 81 5. Tom EX Miller and Aldo Compagnoni. Two-sex demography, sexual niche differentiation, and the geographic range limits
82 of texas bluegrass (poa arachnifera). *The American Naturalist*, 200(1):17–31, 2022.

Table S1. Estimated coefficients for vital rates, including posterior means, 95% credible intervals, the probability of the coefficient being greater than 0, and the probability of the coefficient being less than 0. The coefficients were estimated using a Bayesian mixed-effects model.

Vital rate	Coefficient	mean	2.50%	97.50%	Pr (Coeff >0)	Pr (Coeff <0)
Survival	size*sex	-0.153	-0.543	0.250	0.226	0.774
Survival	sex	-0.382	-1.667	0.838	0.275	0.725
Survival	pptgrow*sex	-0.317	-1.160	0.553	0.232	0.768
Survival	pptdorm*sex	-0.146	-0.855	0.590	0.337	0.663
Survival	tempgrow*sex	-0.431	-1.292	0.428	0.168	0.832
Survival	tempdorm*sex	-0.238	-1.169	0.728	0.311	0.689
Survival	tempdorm*pptdorm*sex	-0.436	-1.135	0.246	0.108	0.892
Survival	tempgrow*pptgrow*sex	0.514	-0.186	1.214	0.649	0.351
Survival	pptgrow2*sex	0.175	-0.394	0.753	0.729	0.271
Survival	pptdorm2*sex	-0.317	-0.743	0.101	0.066	0.934
Survival	tempgrow2*sex	0.351	-0.447	1.166	0.224	0.776
Survival	tempdorm2*sex	-0.204	-0.764	0.349	0.809	0.191
Growth	size*sex	0.169	0.017	0.315	0.983	0.017
Growth	sex	-0.254	-0.753	0.258	0.160	0.840
Growth	pptgrow*sex	0.421	0.070	0.784	0.992	0.008
Growth	pptdorm*sex	-0.212	-0.502	0.079	0.077	0.923
Growth	tempgrow*sex	0.176	-0.155	0.486	0.854	0.146
Growth	tempdorm*sex	-0.308	-0.664	0.036	0.043	0.957
Growth	tempdorm*pptdorm*sex	-0.158	-0.368	0.044	0.069	0.931
Growth	tempgrow*pptgrow*sex	-0.005	-0.314	0.303	0.967	0.033
Growth	pptgrow2*sex	-0.141	-0.317	0.020	0.046	0.954
Growth	pptdorm2*sex	-0.052	-0.209	0.106	0.256	0.744
Growth	tempgrow2*sex	-0.066	-0.367	0.242	0.876	0.124
Growth	tempdorm2*sex	0.105	-0.077	0.277	0.337	0.663
Flowering	size*sex	0.150	-0.277	0.578	0.759	0.241
Flowering	sex	-0.810	-2.324	0.773	0.144	0.856
Flowering	pptgrowsex	-0.087	-1.158	0.934	0.439	0.561
Flowering	pptdormsex	-0.189	-1.052	0.683	0.339	0.661
Flowering	tempgrowsex	-0.215	-1.208	0.783	0.339	0.661
Flowering	tempdormsex	-0.086	-1.164	0.976	0.444	0.556
Flowering	tempdorm*pptdorm*sex	-0.105	-0.701	0.517	0.371	0.629
Flowering	tempgrow*pptgrow*sex	-0.174	-1.192	0.857	0.651	0.349
Flowering	pptgrow2*sex	0.306	-0.214	0.832	0.869	0.131
Flowering	pptdorm2*sex	-0.086	-0.695	0.503	0.394	0.606
Flowering	tempgrow2*sex	-0.348	-1.295	0.545	0.535	0.465
Flowering	tempdorm2*sex	0.022	-0.529	0.552	0.236	0.764
Panicles	size*sex	0.037	-0.088	0.158	0.732	0.268
Panicles	sex	-0.068	-0.340	0.211	0.303	0.697
Panicles	pptgrow*sex	-0.041	-0.289	0.203	0.361	0.639
Panicles	pptdorm*sex	0.010	-0.210	0.233	0.534	0.466
Panicles	tempgrow*sex	0.008	-0.236	0.268	0.514	0.486
Panicles	tempdorm*sex	-0.096	-0.341	0.157	0.229	0.771
Panicles	tempdorm*pptdorm*sex	0.015	-0.207	0.234	0.555	0.445
Panicles	tempgrow*pptgrow*sex	-0.052	-0.287	0.208	0.289	0.711
Panicles	pptgrow2*sex	0.059	-0.153	0.264	0.719	0.281
Panicles	pptdorm2*sex	0.042	-0.148	0.236	0.668	0.332
Panicles	tempgrow2*sex	-0.116	-0.370	0.144	0.173	0.827
Panicles	tempdorm2*sex	-0.092	-0.284	0.100	0.184	0.816